TJNN Thai Journal of Nanoscience and Nanotechnology

Green Light Emission from Tb^{3+} Ion Doped Boro-Tellurite Glass: Potential for Scintillation and Thermoluminescence Material Applications

Seubsakun Khondara[1,2], Patarawagee Yasaka[1,2*], Kitipun Boonin[1,2], and Jakrapong Kaewkhao[1,2]

[1]*Physics Program, Faculty of Science and Technology, Nakhon Pathom Rajabhat University, Nakhon Pathom, 73000, Thailand*
[2]*Center of Excellence in Glass Technology and Materials Science (CEGM), Nakhon Pathom Rajabhat University, Nakhon Pathom, 73000, Thailand*

Received:4 June 2025, Revised: 18 June 2025, Accepted: 20 June 2025

Abstract

Rare-earth doped glasses have gained significant attention due to their potential applications in photonic devices, including scintillators and thermoluminescence dosimeters (TLD). Among these, terbium (Tb^{3+}) ion is known for their strong green luminescence, making them valuable for optical and radiation detection technologies. The combination of TeO_2 and other glass modifiers enhances the optical and structural properties of the host matrix, making it suitable for doping with rare-earth ions. The primary goal of this study is to synthesize and characterize a series of Tb^{3+} doped tellurite-based glasses with varying concentrations of terbium oxide (Tb_2O_3) for scintillation and thermoluminescence material applications. Glasses with the molar composition (30-x) TeO_2: $20B_2O_3$: 20MgO: $10Li_2O$: $10Al_2O_3$: $10La_2O_3$: xTb_2O_3 (x is 0.0, 1.0, 2.0, 3.0, 4.0, and 5.0 mol%) were produced using a conventional melt-quenching approach. X-ray diffraction analysis confirmed that the glass was amorphous. In addition, the UV-VIS-NIR spectrometer recorded the absorption spectra of a number of peaks. As the concentrations of Tb^{3+} increase, both the radioluminescence (RL) and photoluminescence (PL) results increase. The glass samples exhibited strong luminescence spectra with prominent emission bands at 545 nm, corresponding to the characteristic transitions of the Tb^{3+} ion. The highest luminescence efficiency of the Tb^{3+} ion was observed at a concentration of 4 mol%. In the prepared glasses, the RL and PL obtained from different concentrations of Tb^{3+} ions are almost close to the green light region, as shown in the CIE 1931 chromaticity diagram. Furthermore, the thermoluminescence (TL) parameters were calculated using Chen's peak shape method, such as activation energy (E) and frequency factor (S). The developed glasses show promise for use in Scintillation and TLD.

Keywords: Tellurite Glass, Photoluminescence, Radioluminescence, Thermoluminescence, Terbium oxide

1. Introduction

Radiation has valuable applications in various fields, including science, industry, agriculture, and medicine, providing numerous benefits. However, its use is accompanied by inherent risks due to its invisible and intangible nature. The potential impact of these risks is closely tied to the level of exposure. Devices like dosimeters have been established to monitor radiation levels in order to ensure safety. These tools play a vital role in safeguarding healthcare professionals and others working with radiation-emitting equipment, helping to maintain exposure within safe and acceptable limits [1]. Optically Stimulated Luminescence Dosimeters (OSLDs) and Thermoluminescent Dosimeters (TLDs) are commonly used to measure radiation exposure. This study places particular emphasis on thermoluminescence materials (TLMs). The concept of TL is founded on the ability of certain materials to emit luminescence upon being heated, a response to their previous exposure to radiation [2], [3].

Thermoluminescence (TL) is one of the most widely used research techniques applied in various fields, particularly in radiation dosimetry. However, this technique has several disadvantages, including a complex luminescence curve structure, loss of sensitivity upon reuse, and the retention of residual signals. Therefore, there is significant potential for developing new and more efficient materials for

Corresponding Author: pyasaka@hotmail.com, pyasaka@webmail.npru.ac.th

personal dosimetry using TL. In recent years, extensive research has been conducted on rare-earth-doped materials, which are considered promising candidates for a variety of advanced applications. These materials are crucial for radiation detection due to their excellent luminescence efficiency and dose response, achieved by incorporating rare-earth ions into a suitable host matrix. Compared to materials without rare-earth doping, their luminescent properties primarily arise from the 4f–4f and 4f–5d electron transitions of RE^{3+} ions. Among these, the 4f–4f transitions are particularly notable for their sharp and well-defined emission bands, spanning from the ultraviolet to the infrared region. This behavior is attributed to the shielding effect of the outer 5s and 5p electrons on the 4f orbitals [4], [5]. Among rare-earth ions, the Tb^{3+} ion exhibits exceptional emission properties. Specifically, they serve as highly efficient green luminescence centers, emitting at 545 nm through transitions between the $^5D_4$ and $^7F_5$ energy levels. This makes Tb^{3+} a promising candidate for a wide range of applications. Furthermore, Tb^{3+} ions tend to form deep trap centers within the host material, leading to thermally stable TL peaks at relatively high temperatures, an advantageous feature for radiation dosimetry applications [6].

Considering these factors, many researchers in recent years, particularly those focused on developing rare-earth TL materials, have explored them as alternatives to existing dosimetry systems. However, most of these studies lack systematic investigations, such as detailed analyses and calculations of key parameters needed to understand TL behavior induced by thermal excitation following prior irradiation. In TL studies, the emission intensity of a material is monitored while it is gradually heated. This process generates a thermoluminescence (TL) glow curve, which maps the variation in luminescence intensity as a function of temperature. The peaks observed on this curve correspond to specific energy levels associated with charge carriers trapped within the material. These glow curves are critical for evaluating the suitability of a material for dosimeter applications. When radiation interacts with defects in the material, it can result in charge trapping and subsequent release mechanisms. To analyze TL behavior, a well-established analytical technique known as Chen's peak shape method is often employed. This method enables the determination of kinetic parameters such as the kinetic order, activation energy, and frequency factor of TL peaks.

This research investigates the effects of Tb^{3+} ion doping on the physical, structural, optical, photoluminescence, irradiance, and thermoluminescence properties of lanthanum–aluminum–lithium–magnesium–boro–tellurite glasses. This glass system was selected as the host matrix due to its excellent optical transparency and favorable physical and mechanical properties. It demonstrates high strength, good resistance to deformation, and versatile fabrication characteristics, making it suitable for use in compact thermoluminescence material (TLM) dosimetry applications. The glass was prepared via primary annealing at high temperatures, followed by rapid quenching to form an amorphous glass network. Tellurium oxide (TeO_2) was used as the primary glass-forming oxide due to its high refractive index, low melting point, high rare-earth ion solubility, and low phonon energy, all of which are essential for efficient luminescence [7], [8]. Additionally, boron oxide (B_2O_3) contributes to structural stability and enhances thermal durability, which are crucial for ensuring the long-term performance and reliability of dosimetry materials under practical conditions [9].

2. Experimental

In this research, glasses with the combinations $(30\text{-}x)TeO_2\text{-}20B_2O_3\text{-}20MgO\text{-}10Li_2O\text{-}10Al_2O_3\text{-}10La_2O_3\text{-}xTb_2O_3$ (x = 0.00, 1.00, 2.00, 3.00, 4.00, and 5.00 mol%) were prepared using a conventional melt-quenching approach. The chemicals used were of high purity, namely tellurium oxide: 99.8%, boric acid: 99.8%, magnesium carbonate: 99.0%, lithium carbonate: 99.0%, aluminum oxide: 99.0%, lanthanum oxide: 99.9%, and Terbium oxide: 99.9%.

Fifteen grams of chemicals, prepared according to the compositions listed in Table 1, were weighed and melted in porcelain crucibles using an electric furnace. The temperature was gradually increased from room temperature to 1100 °C at a controlled rate of 5 °C per minute. After reaching 1100 °C, the melt was held at this temperature for 1 hour to ensure complete melting and homogeneous mixing of the glass constituents. The molten glass was then poured onto a preheated graphite plate and annealed at 350 °C for 3 hours to relieve internal stresses. After annealing, the glass was slowly cooled to room temperature (as show in Fig. 1). The resulting solidified glass was then cut and polished into two sample sizes, 1.0 × 1.5 × 0.3 and 0.5 × 0.5 × 0.1 cm^3, for various property evaluations.

The glass samples were thoroughly characterized to evaluate their physical, optical, and structural properties using various analytical instruments. Density was measured using an AND HR-200 instrument, while the refractive index was determined with a Presidium Refractive Index Meter II. Structural analysis was conducted using a Rigaku Smart Lab X-ray diffractometer (XRD). Vibrational and absorption characteristics of the glass network were investigated using a Nicolet™ iS™5 FTIR spectrophotometer and a Shimadzu UV-3600 UV-Vis-NIR Spectrometer. Luminescence properties were measured using a Hitachi fluorescence spectrometer. The photoluminescence quantum yield (PLQY) was determined using a PerkinElmer FL8500 Fluorescence Spectrophotometer equipped with an integrating sphere and a Xenon light source. Thermoluminescence (TL) characteristics were studied following gamma irradiation with a ^{241}Am source, using a TLD Reader-Analyzer (Model RA04400).

Table 1. Chemical composition of the prepared glasses.

Glass Codes	Composition (mol%)						
	TeO_2	B_2O_3	MgO	Li_2O	Al_2O_3	La_2O_3	Tb_2O_3
Tb0.0	30.0	20.0	20.0	10.0	10.0	10.0	0.0
Tb1.0	29.0	20.0	20.0	10.0	10.0	10.0	1.0
Tb2.0	28.0	20.0	20.0	10.0	10.0	10.0	2.0
Tb3.0	27.0	20.0	20.0	10.0	10.0	10.0	3.0
Tb4.0	26.0	20.0	20.0	10.0	10.0	10.0	4.0
Tb5.0	25.0	20.0	20.0	10.0	10.0	10.0	5.0

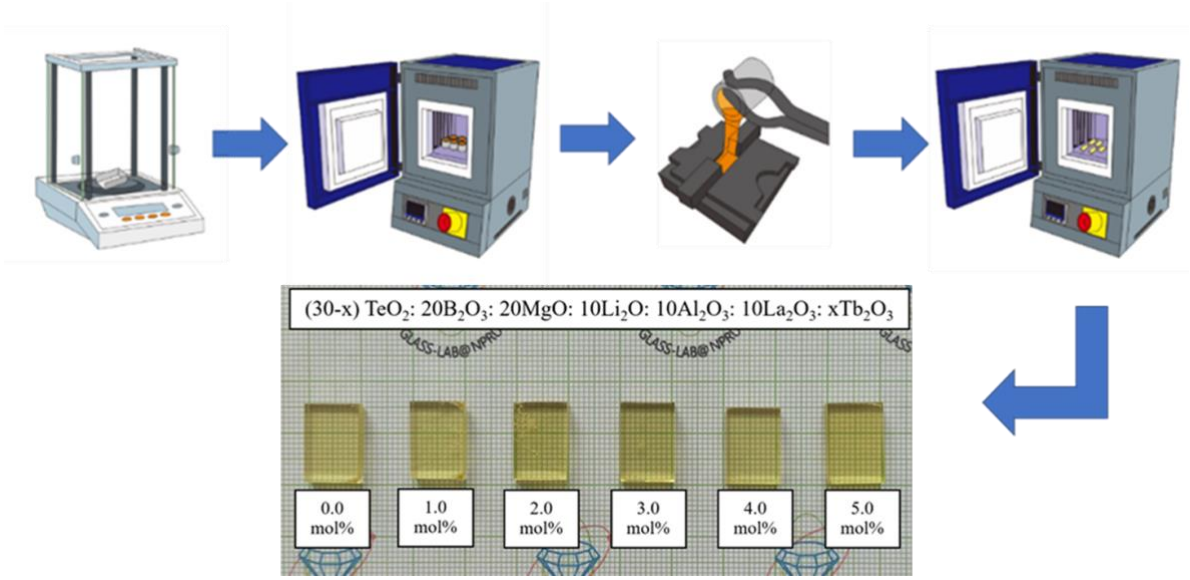

Fig. 1. Preparation of glass samples.

3. Result and discussion

3.1 Density, Molar volume, and Refractive index

The analysis of glass structure is intricately linked to its density and molar volume, both of which are fundamental parameters crucial for investigating a broad spectrum of properties. The following formula can be used to determine the density of the glasses:

$$\rho_{glass} = \frac{W_a}{W_a - W_w} \times \rho_w \quad (1)$$

where W_a stands for the weight of the glass in air, the weight of the glass in water is represented by W_w, and ρ_w is the density of water (0.997 g/cm^3). The molar volume of glass can be calculated using the following formula:

$$V_m = \frac{M_T}{\rho_{glass}} \quad (2)$$

where V_m (cm^3/mol) is molar volume, M_T (g/mol) is the sum of molecular masses, and ρ_{glass} (g/cm^3) is density. Fig. 2 demonstrates the effect of varying Tb_2O_3 concentrations on the prepared glass ρ, V_m, and refractive index (n). The experimental results reveal that the density increases gradually with the concentration of Tb_2O_3. In contrast, the molar volume generally tends to decrease with the increase of Tb_2O_3 content, reflecting the inverse relationship between ρ and V_m. The refractive index, which often correlates with material density, showed variations as Tb_2O_3 content was altered. Materials with higher densities generally have higher refractive indices. These trends are likely due to structural modifications within the glass network induced by the Tb^{3+} ion, which is heavier and larger than the ions in the base glass. The addition of Tb^{3+} ions disrupts the network, occupying more space, and leading to changes in ρ, V_m, and n.

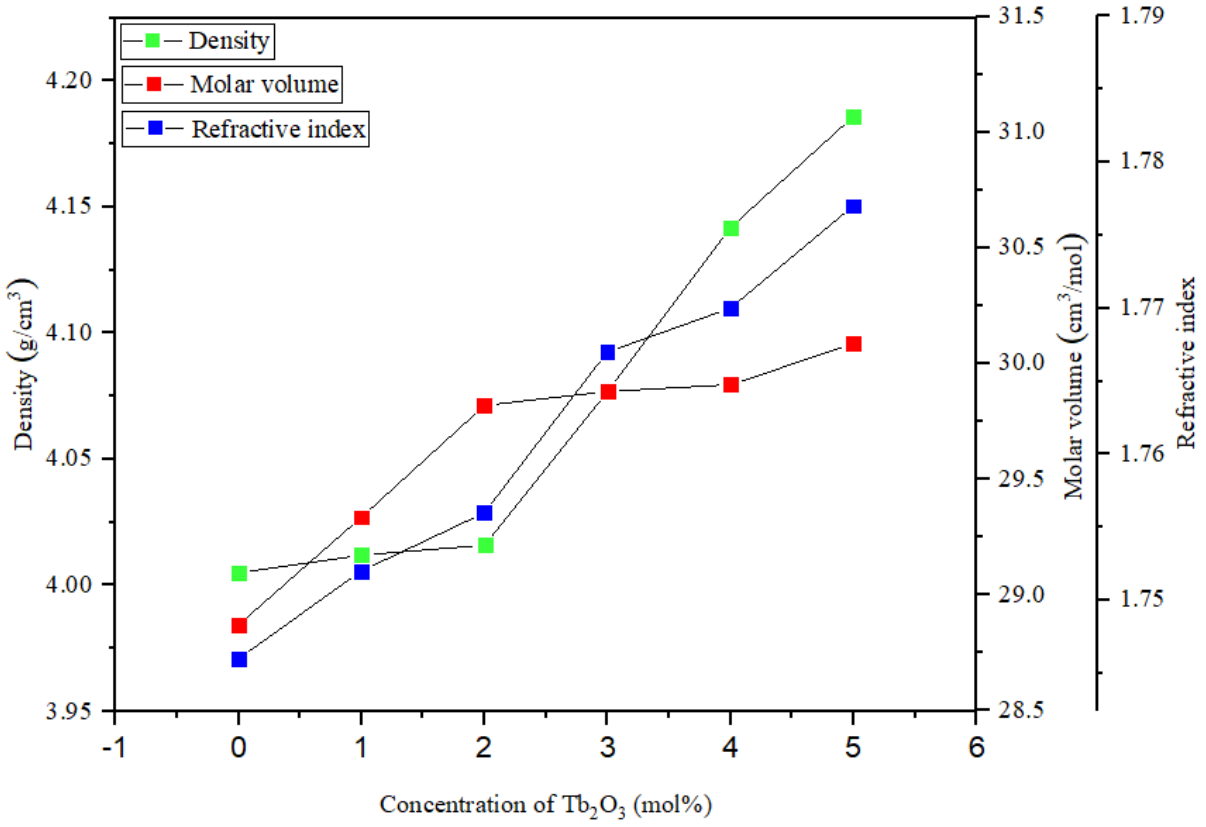

Fig. 2. Density, molar volume, and refractive index of glass samples doped with various Tb_2O_3 concentrations.

3.2 X-ray diffraction (XRD) analysis

The amorphous nature of the glasses is confirmed by the patterns of XRD displayed in Fig. 3. A scan speed of 5°/min was used to examine Bragg angles from 10° to 80° during the measurements, which were carried out using Cu Kα radiation at 40 kV and 30 mA. The XRD spectra indicate that the glass is amorphous, as there are no strong peaks, signifying the absence of long-range order found in crystalline structures. This result is consistent with characteristics commonly reported for similar glass systems. The absence of distinct crystalline features is a key property of the glass network, making it possible for applications that demand consistent material properties and stability. The broad halo formed in the XRD reflects the disordered arrangement of the glass structure.

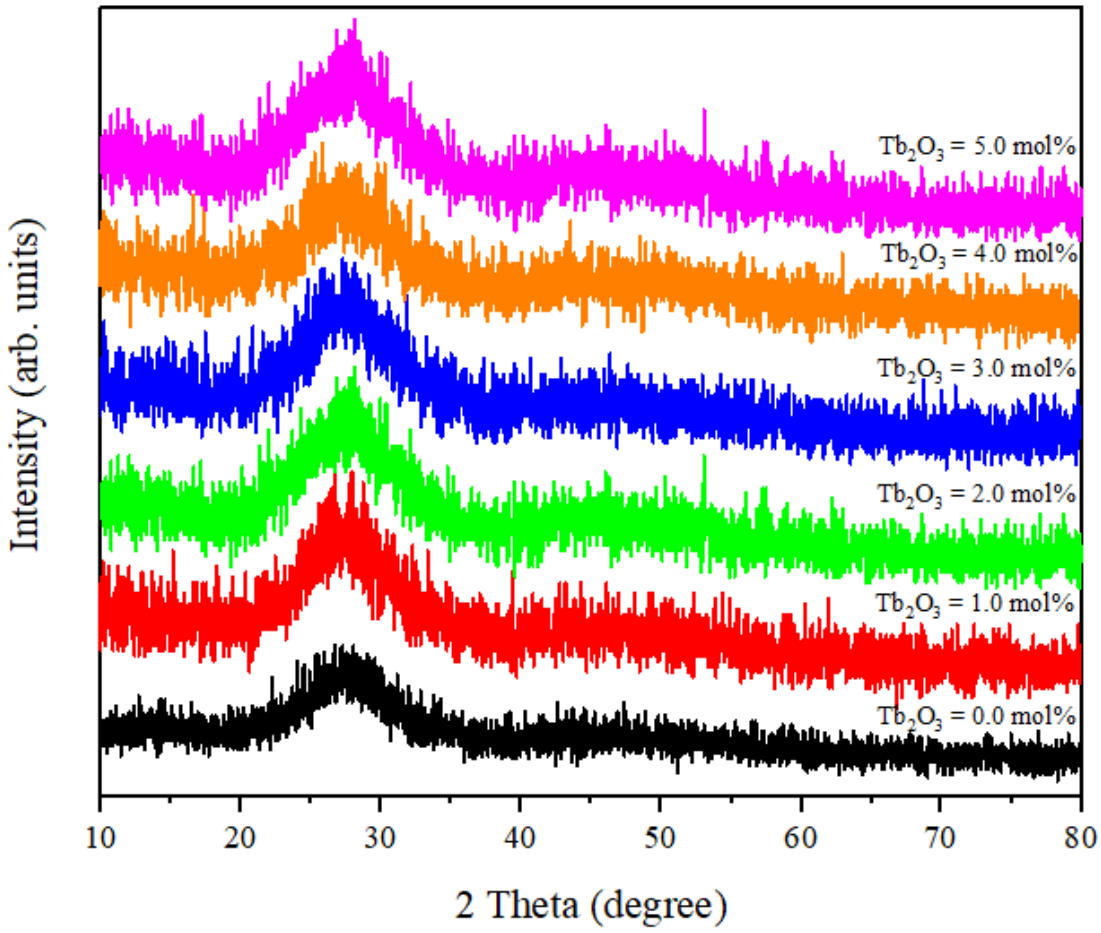

Fig. 3. XRD pattern of glass doped with various Tb_2O_3 concentrations.

3.3 Fourier transform infrared spectroscopy (FTIR)

Fig. 4 shows the FTIR spectra of the glasses, recorded in the 400 to 4000 cm^{-1} wavenumber regions to analyze the vibrational characteristics of the glass network. Four prominent vibrational bands were identified at 650, 905, 1220, and 2920 cm^{-1}. The 650 cm^{-1} band represents the Te-O-Te bond stretching vibrations in the TeO_4 structural unit, while the 905 cm^{-1} band signifies B-O bonds in the BO_4 unit. The 1220 cm^{-1} peak denotes B-O bond stretching in BO_3 groups, and the 2920 cm^{-1} band relates to O-H group stretching vibrations (as shown in Table 2). The presence of O-H groups in the glass matrix is significant, as they can act as quenching centers for luminescence by facilitating non-radiative energy loss (check the sentence). This characteristic can influence the efficiency of optical applications. The observed vibrational bands provide insights into the glass structure, highlighting the contributions of boron and tellurium oxide units in the formation of the glass network [10].

Table 2. Mode of vibration from FTIR spectra of the prepared glass samples.

Wavenumber (cm^{-1})	Assignments	Reference
650	Stretching vibrations of TeO_4 units.	[11]
905	Stretching vibrations of BO_4 units.	[12]
1220	Stretching vibrations of BO_3 units.	[12]
2920	Stretching vibrations of OH groups.	[10]

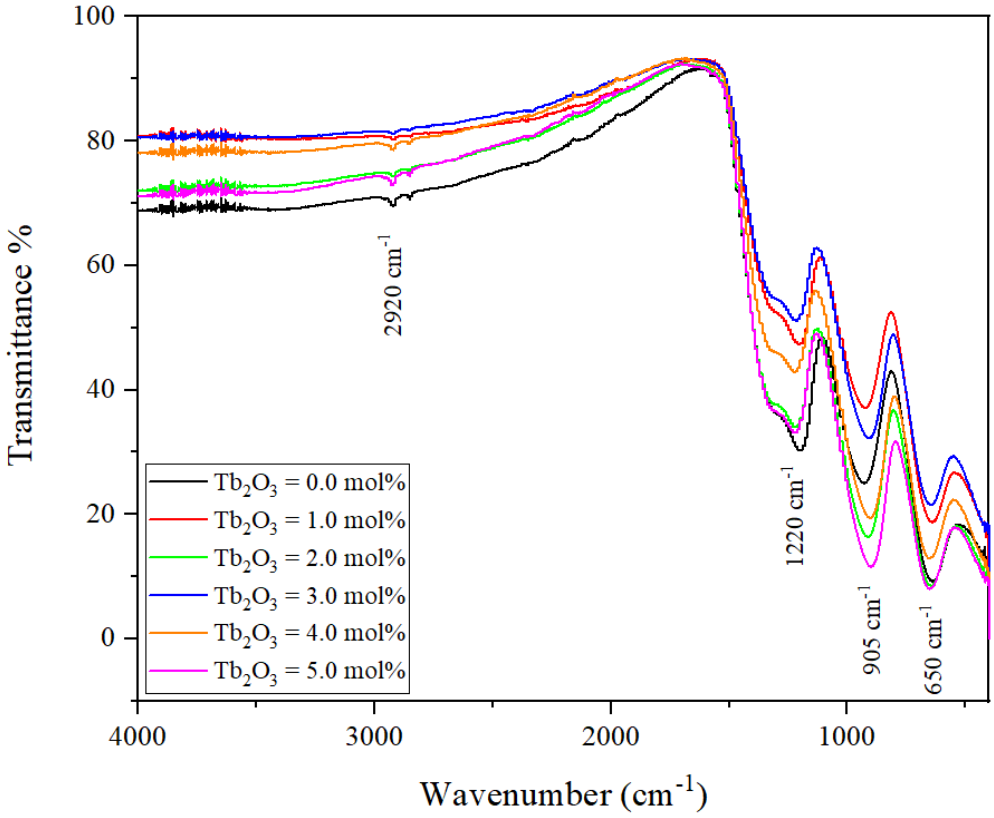

Fig. 4. FTIR spectra of glass samples doped with various Tb_2O_3 concentrations.

3.4 Absorption spectra

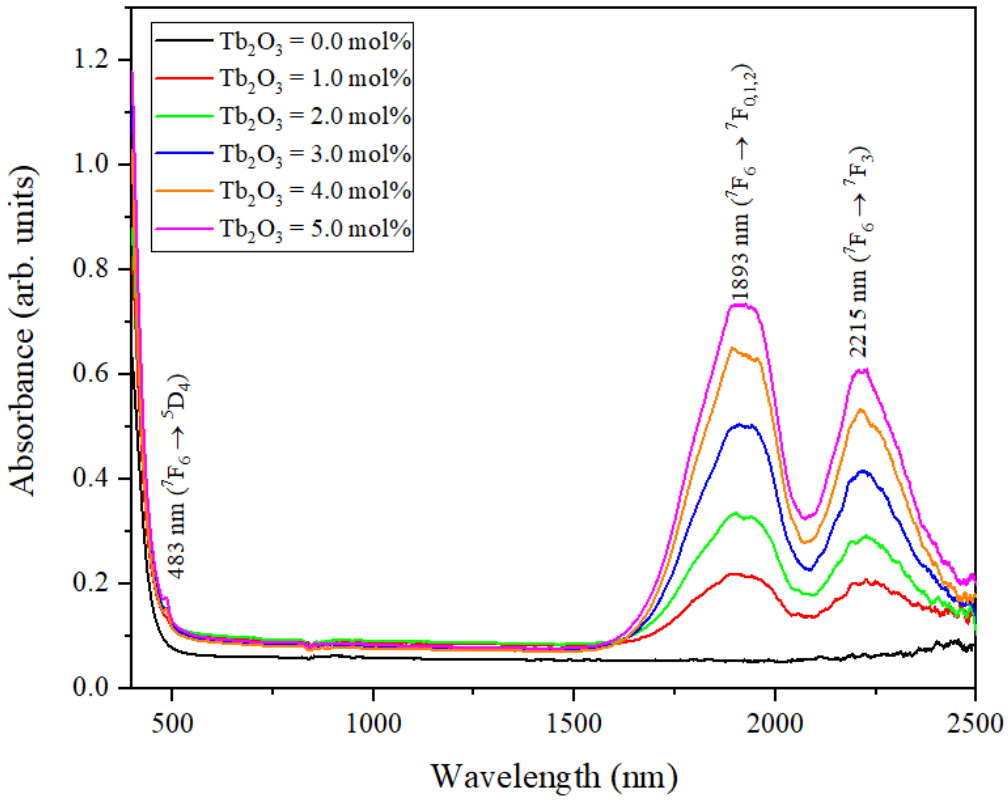

Fig. 5. The absorbance spectra of glass doped with Tb_2O_3 concentration.

Fig. 5 shows the prepared glasses' absorption spectra, which were measured from 400 to 1900 nm in the wavelength range. The undoped glass exhibited no distinct absorption peaks, indicating a lack of significant optical transitions. In contrast, the Tb_2O_3-doped glasses revealed multiple absorption peaks in the near-infrared region at 483, 1893, and 2215 nm. These peaks represent Tb^{3+} ion transitions from ground state $^7F_6$ to the excited states $^5D_4$, $^7F_{0,1,2}$, and $^7F_3$, respectively [13], [14]. As the Tb_2O_3 concentration increased, the intensity of these absorption peaks also increased, indicating stronger optical transitions. This enhancement is due to the increasing population of Tb^{3+} ions, which introduce additional energy levels within the bandgap of the glass matrix. The observed absorption behavior of glass indicates the influence of Tb_2O_3 doping on the glass.

3.5 Photoluminescence (PL) studies

The excitation spectra of Tb_2O_3 doped glass recorded from 200-600 nm wavelength range under an emission at 545 nm as shown in Fig. 6(a). The spectra exhibit peaks at 285, 319, 342, 354, 369, 378, and 486 nm, corresponding to the transitions of the Tb^{3+} ion: $^7F_6 \rightarrow {}^5H_7$, $^5L_6$, $^5L_9$, $^5L_{10}$, ($^5G_6$+$^5D_3$), and $^5D_4$, respectively [13], [14]. Among these transitions, the peak at 486 nm exhibits the highest intensity, indicating that it is the most effective excitation wavelength for promoting the Tb^{3+} ion to the $^5D_4$ excited state. This makes 486 nm the preferred excitation wavelength for further emission studies. Fig. 6(b) displays the PL spectra of Tb_2O_3 doped glass measured from 450-650 nm under excited at 486 nm. The spectra exhibit peaks at 488, 545, 585, and 622 nm, corresponding to the electron transitions of the Tb^{3+} ion: $^5D_4 \rightarrow {}^7F_6$, $^7F_5$, $^7F_4$, and $^7F_3$, respectively [13], [14]. Among these transitions, the green peak emission at 545 nm was the most intense. The photoluminescence intensity increased with Tb_2O_3 concentration up to 4.0 mol%. At this optimal concentration, energy transfer between Tb^{3+} ions is minimal, and the emission efficiency is maximized. However, beyond 4.0 mol%, the luminescence intensity starts to decrease as a result of the concentration quenching effect [15]. This phenomenon occurs when Tb^{3+} ions are packed too closely together; as a result, non-radiative energy transfer occurs between neighboring ions. This energy transfer reduces the probability of radiative transitions, leading to a decrease in overall luminescence intensity. The quantum yield (QY) of Tb_2O_3-doped borotellurite glass was measured for the sample that exhibited the highest photoluminescence intensity, which corresponded to a doping concentration of 4.0 mol% Tb_2O_3. The measurement was performed under an excitation wavelength of 486 nm, as depicted in Fig. 7. The quantum yield, expressed as the percentage of emitted photons relative to absorbed photons, was calculated to be 15.22% for the 4.0 mol% Tb_2O_3 sample and the energy level diagram of Tb_2O_3-doped glass shown in Fig. 8.

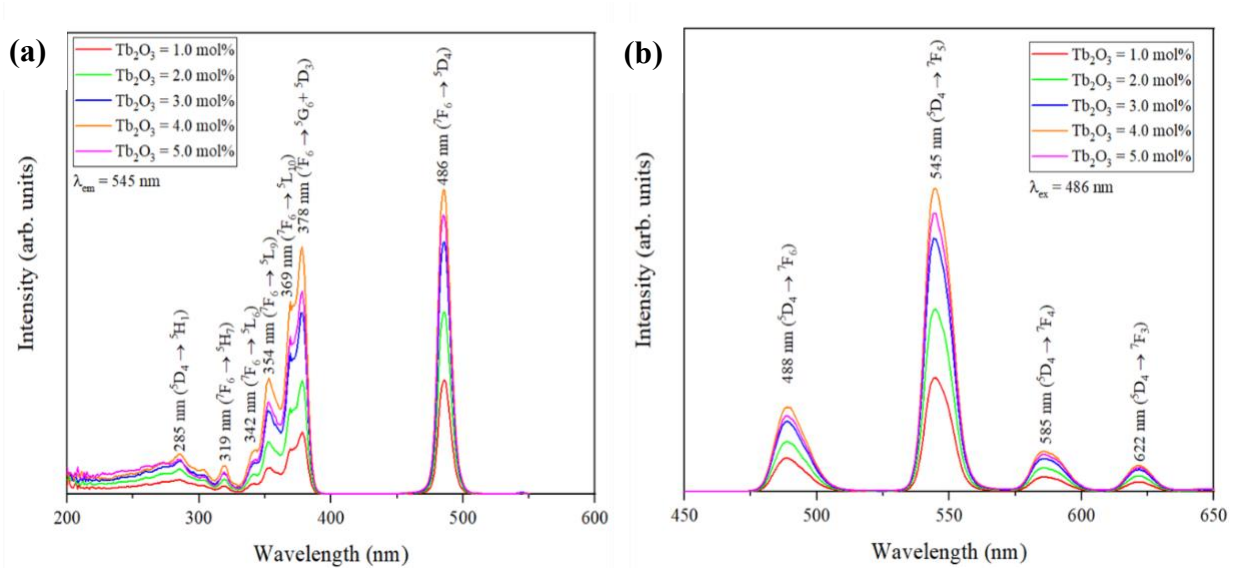

Fig. 6. (a) Excitation spectra, and (b) Emission spectra of glass doped with Tb_2O_3 concentration.

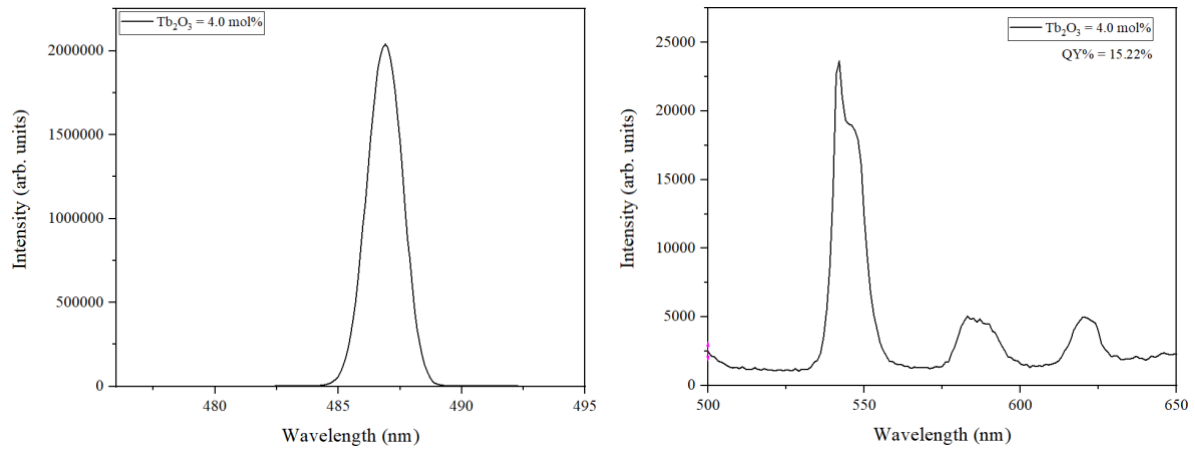

Fig. 7. Quantum yield of glass doped with Tb_2O_3 concentration.

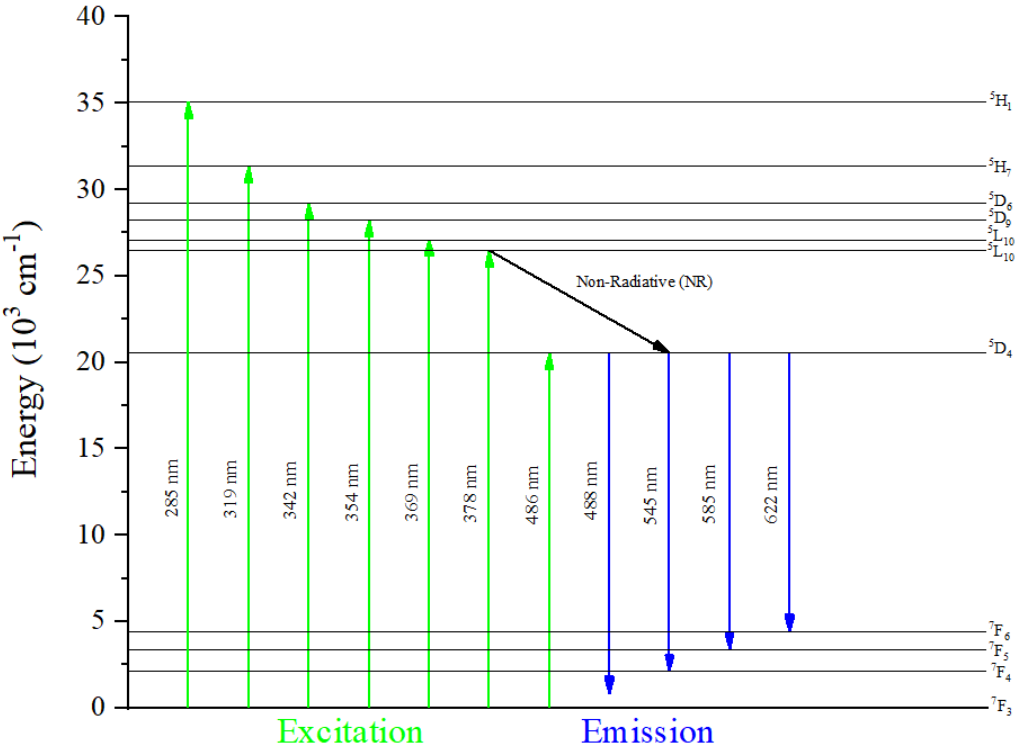

Fig. 8. Energy level diagram of Tb_2O_3-doped glass.

The CIE 1931 chromaticity diagram, as in Fig. 9, was employed to evaluate the color characteristics of the luminescence emitted by Tb_2O_3-doped glasses under 486 nm excitation. The chromaticity coordinates, calculated from the emission spectra, were plotted on the diagram. These coordinates fall within the green light region, indicating that the glasses are capable of emitting balanced green light, a desirable property for applications in green light-emitting diodes. The color purity of a glass can be evaluated by [16]:

$$Color\ purity = \frac{\sqrt{(x-x_i)^2+(y-y_i)^2}}{\sqrt{(x_d-x_i)^2+(y_d-y_i)^2}} \times 100\% \quad (3)$$

where (x, y) are the CIE coordinates of glass, (x_i, y_i) are CIE coordinates of the standard white illumination (0.313, 0.329), and (x_d, y_d) are CIE coordinates at the dominant wavelength for glass were estimated as (0.266, 0.724) respectively. And Table 3 presented the CIE1931 color coordinates, and color purity parameters of glass dope Tb_2O_3.

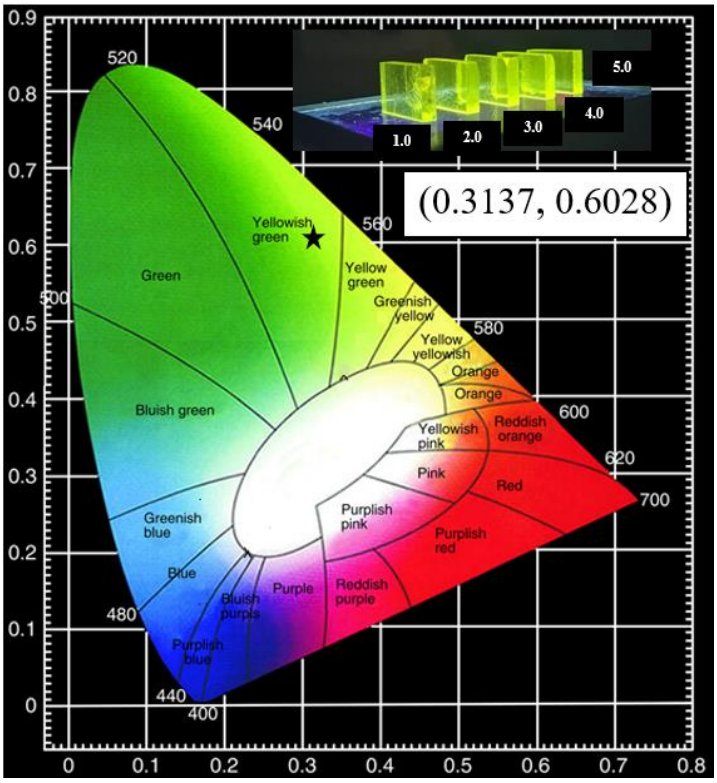

Fig. 9. The CIE 1931 diagram of glass doped with Tb_2O_3 concentration and a photograph of all glasses illuminated by a UV lamp at 365 nm.

Table 3. CIE1931 color coordinates, and color purity parameters of glass dope Tb_2O_3

Glass Codes	CIE1931		Color purity (%)
	x	y	
Tb1.0	0.3106	0.6023	68.6978
Tb2.0	0.3132	0.6041	69.1687
Tb3.0	0.3137	0.6034	68.9697
Tb4.0	0.3137	0.6028	68.8390
Tb5.0	0.3148	0.6034	68.9717

The decay profiles were fitted to a single exponential function, revealing the characteristic lifetime of the $^5D_4 \rightarrow {}^7F_5$ transition of the Tb^{3+} ion, as shown in Fig. 10. The observed decay times decreased with increasing Tb_2O_3 concentration, suggesting the influence of energy transfer processes at higher doping levels. At lower Tb_2O_3 concentrations, the decay times were relatively longer due to the isolated nature of the Tb^{3+} ion, which minimized non-radiative processes. However, as the concentration of Tb_2O_3 increased, the Tb^{3+} ions were brought closer together, enhancing cross-relaxation and energy migration mechanisms. These non-radiative processes lead to a faster depletion of the excited state, resulting in shorter decay times. The decrease in decay time at higher Tb_2O_3 concentrations suggests concentration quenching, where energy is transferred between closely spaced Tb^{3+} ions instead of being radiatively emitted. This effect is a crucial consideration in designing materials for luminescence applications, as it imposes a limit on the optimal doping concentration. The decay time behavior also highlights the efficiency of the Tb^{3+} ion as luminescence centers within the glass matrix. At the optimal concentration of 4.0 mol% Tb_2O_3, the decay time was long enough to support strong emission without significant quenching effects, making the glass suitable for optical applications like green light-emitting devices. Beyond this concentration, the rapid decrease in decay time diminishes the luminescence performance, emphasizing the importance of optimizing ion distribution within the glass network.

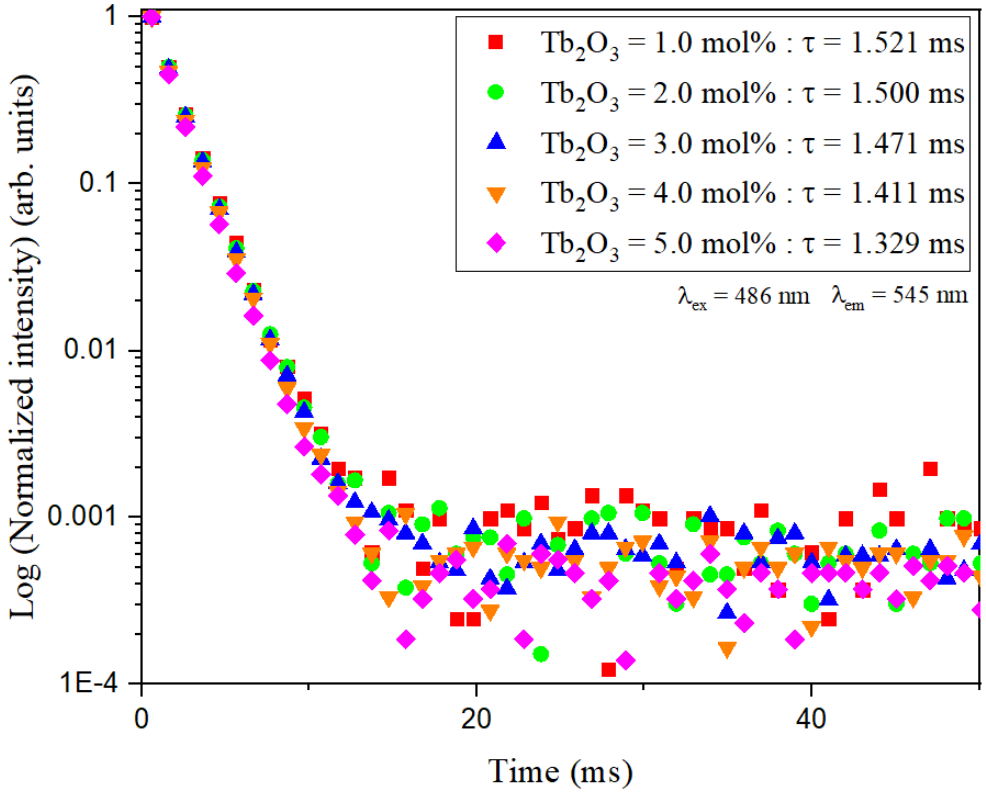

Fig. 10. The luminescence decay time of glass doped with Tb_2O_3 concentration.

3.6 Radioluminescence (RL)

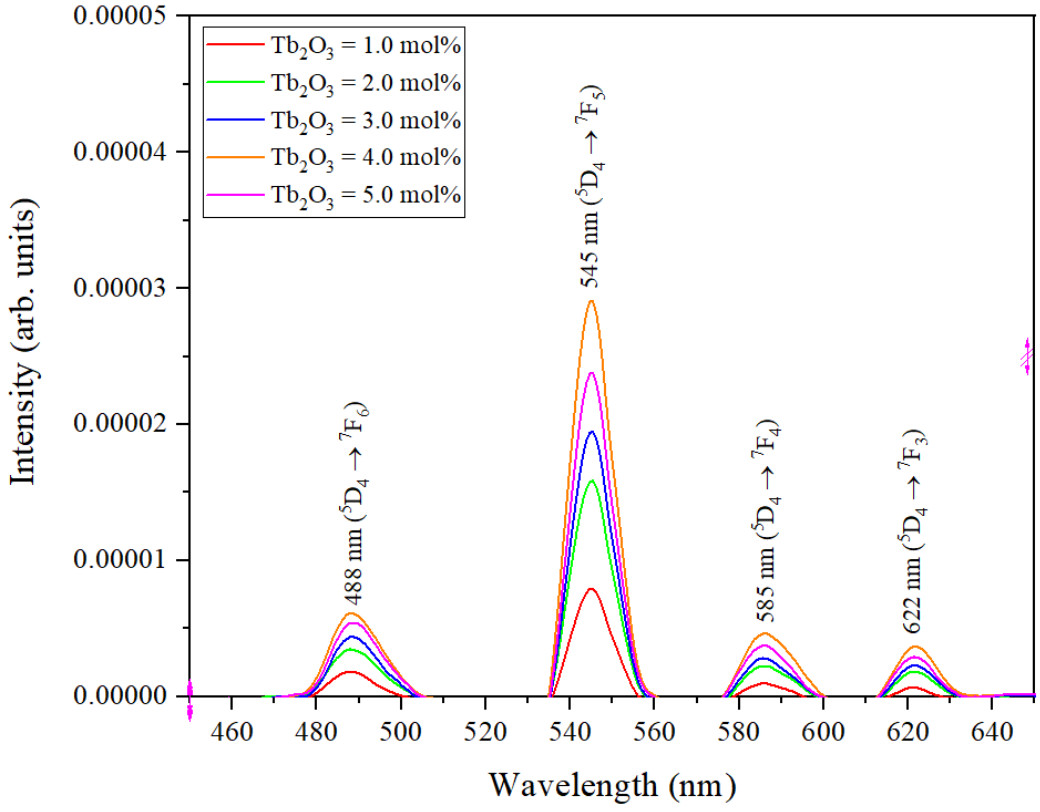

Fig. 11. The radioluminescence of glass doped with Tb_2O_3 concentration.

The Radioluminescence (RL) is a powerful technique for evaluating the emission properties of materials exposed to high-energy radiation, such as X-rays or gamma rays. This method is particularly effective for investigating luminescent materials, as it reveals the influence of local environmental asymmetry around the Tb^{3+} ion on their emission behavior. The RL spectrum was monitored using the Cu target X-ray generator (Inel, XRG3D-E) operated with 50 kV and 30 mA power and the optical fiber - spectrometer (Ocean Optics, QE65 Pro), as illustrated in Fig.11. The spectra exhibit peaks at 488, 545, 585, and 622 nm, corresponding to the electron transitions of Tb^{3+} ion: $^5D_4 \rightarrow {}^7F_6$, $^7F_5$, $^7F_4$, and $^7F_3$, respectively. These emission features closely resemble those observed in the photoluminescence (PL) spectra, indicating similar underlying excitation and relaxation mechanisms.

3.7 Thermoluminescence (TL)

The thermoluminescence (TL) characteristics of Tb_2O_3-doped boro-tellurite glasses were examined following gamma irradiation at a dose of 1.5 mGy from a ^{241}Am source. The TL glow curves were recorded at a constant heating rate of 5 °C/s up to 300 °C. As shown in Fig. 12, it can be seen that the TL glow peak of the undoped glass (Tb_2O_3 = 0.0 mol%) appears at a lower temperature compared to the Tb_2O_3-doped samples. The slight shift of the TL peak toward higher temperatures with increasing Tb_2O_3 concentration, a prominent glow peak appeared between 248°C and 251°C for all Tb_2O_3 concentrations, indicating the presence of stable trapping centers in the glass matrix. The variations observed in the peak position, shape, and intensity with changing Tb_2O_3 concentrations suggest that the Tb^{3+} ion significantly influences the electron trapping and de-trapping processes. These glow curves result from the thermally stimulated release of electrons from radiation-induced traps, followed by recombination at luminescent centers. To investigate the kinetic behavior of the TL peaks, Chen's peak shape method, a well-established analytical technique, was employed [17].

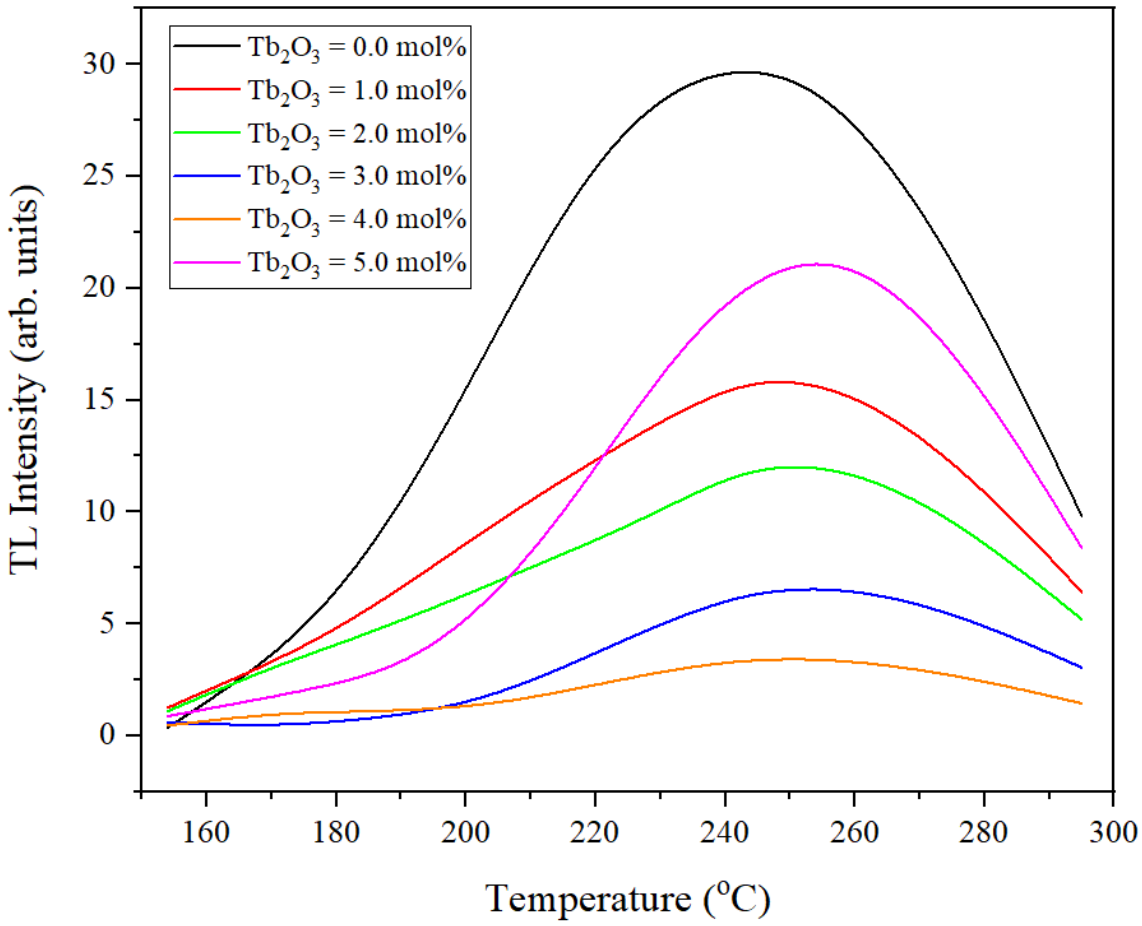

Fig. 12. The TL glow curves of glass dope with Tb_2O_3 concentration.

This method allows the determination of kinetic parameters, including activation energy (E), maximum peak temperature (T_M), and frequency factor (S), without the need for iterative procedures or prior assumptions regarding kinetic order. Key parameters derived from the TL glow curves include: T_1 and T_2 temperatures at half-maximum intensity (rising and falling edges), τ (defined as T_M-T_1), which is the half-width on the increasing side, δ (defined as T_2-T_M), which is the half-width on the decreasing side, ω (defined as T_2-T_1), which is the total half-width, and μg (defined as δ/ω), which is the geometrical shape factor that reflects the kinetic order of the glow peak. The symmetry factor (μ_g) provides insight into the kinetic order of TL peaks, with μg ≈ 0.42 and 0.52 indicating first-order and second-order kinetics, respectively. The values of τ, δ, ω, and μg for each sample are presented in Table 4, while Fig. 13 illustrates the key points defining the glow peak geometry. The activation energy values, calculated according to Chen's equations, are summarized in Table 5. These values, ranging from 0.52 to 0.94 eV, represent the minimum energy required for trapped charge carriers to escape their traps. The average activation energy (E_α) was computed as the mean of E_τ, E_δ, and E_ω, offering a more holistic understanding of the trap depth characteristics for each sample. The equations can be summarized as follows [17]:

$$E_\alpha = c_\alpha\left(\frac{kT_M^2}{\alpha}\right) - b_\alpha(2kT_M) \tag{5}$$

Where α is τ, δ, or ω. The values of c_α and b_α are summarized below:

$$c_\tau = 1.51 + 3.0(\mu_g - 0.42)\ ;\ b_\tau = 1.58 + 4.2\left(\mu_g - 0.42\right)$$

$$c_\delta = 0.976 + 7.3(\mu_g - 0.42)\ ;\ b_\delta = 0$$

$$c_\omega = 2.52 + 10.2(\mu_g - 0.42)\ ;\ b_\omega = 1$$

In TL, the frequency factor is a crucial parameter that describes the probability of trapped electrons or charge carriers escaping from their traps as the material is heated. It plays a role similar to the pre-exponential factor in the Arrhenius equation, but it is specifically applied to processes involving the release of trapped charge carriers in crystalline or amorphous materials under thermal stimulation. The frequency factor can be obtained using the following formula [17]:

$$S = \frac{\beta E}{kT_M^2\left[1+(b-1)\left(\frac{2kT_M}{E}\right)\right]} exp\left(\frac{E}{kT_M}\right) \tag{6}$$

Where β (K/s) is the constant heating rate
k (eV/K) is the Boltzmann constant

Table 4. Calculated TL parameter of glass dope Tb_2O_3

Glass Codes	T_M (K)	T_1 (K)	T_2 (K)	T (K)	Δ (K)	ω (K)	μ_g	FOM%
Tb0.0	516.15	471.99	560.15	44.16	44.00	88.16	0.50	1.47
Tb1.0	524.15	476.35	568.15	47.80	44.00	91.80	0.48	2.99
Tb2.0	521.15	472.37	566.15	48.78	45.00	93.78	0.48	2.95
Tb3.0	526.00	489.00	568.00	37.00	42.00	79.00	0.52	2.66
Tb4.0	526.00	436.00	568.00	90.00	42.00	132.00	0.32	>3.5
Tb5.0	527.15	489.79	564.15	37.36	37.00	74.36	0.50	1.91

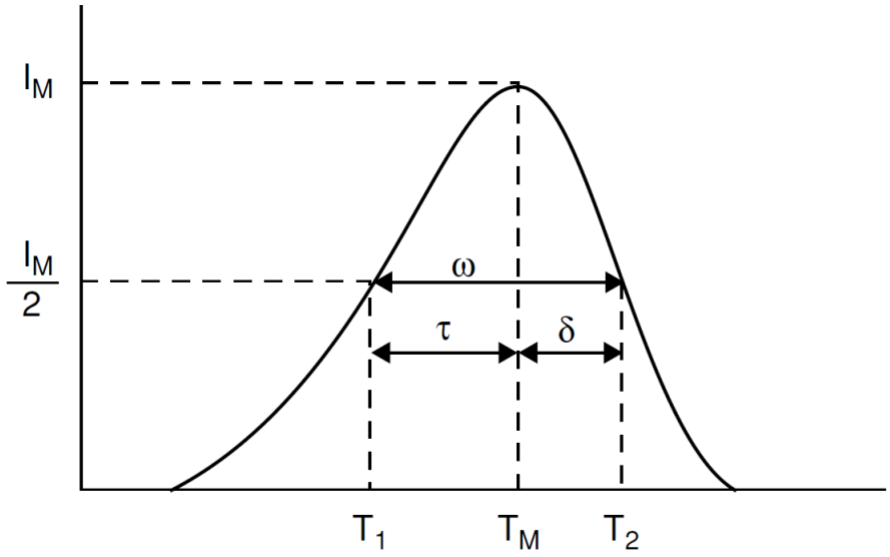

Fig. 13. The characteristic points on a TL glow curve, which define the peak-shape parameters

Table 5. Calculated activation energy values

Glass Codes	E_ω (eV)	E_τ (eV)	E_δ (eV)	E_α (eV)
Tb0.0	0.78	0.74	0.81	0.78
Tb1.0	0.72	0.67	0.76	0.71
Tb2.0	0.69	0.65	0.73	0.69
Tb3.0	1.01	1.00	1.02	1.01
Tb4.0	0.18	0.21	0.13	0.17
Tb5.0	0.98	0.94	1.00	0.97

The computed frequency factor values for both first- and second-order kinetics are shown in Table 6. These span several orders of magnitude and provide insights into the thermal stability and release probability of trapped carriers. In the accuracy assessment of glow curve deconvolution, the Figure of Merit (FOM) is used to quantify the goodness of fit between the experimental thermoluminescence (TL) data (TL_{exp}) and the theoretically best-fitted values (TL_{fit}). The FOM serves as a performance indicator, enabling a straightforward comparison of fitting quality by consolidating key error parameters into a single value. Calculating the value of the FOM for all the TL glow peaks, where, if the FOM values are between 0.0% and 2.5%, indicates a good fit, 2.5% and 3.5% indicates a slight deviation or minor fitting flaw, and > 3.5% indicates a poor fit. The calculated FOM values were between 1.47% and 2.99%, indicating good FOM compatibility, with only minor deviations in some cases [18], [19].

$$FOM = \frac{\Sigma|TLfit_{exp}||}{\Sigma TL_{fit}} \quad (7)$$

The distinct TL glow peaks, combined with consistent kinetic parameters, indicate that Tb_2O_3-doped boro-tellurite glasses exhibit stable and reliable TL behavior. The ability to tailor the TL response by varying Tb_2O_3 concentration further enhances the suitability of these materials for radiation dosimetry applications. Comparative analysis with previous studies. To evaluate the effectiveness of the Tb_2O_3-doped tellurite-borate glass system investigated in this study, a comparison with other rare-earth-doped glasses reported in the literature**.** Parameters such as activation energy (E), maximum peak temperature (T_m), and frequency factor (S)are considered. The comparison shows that the (30-x)TeO_2-20B_2O_3-20MgO-10Li_2O-10Al_2O_3-10La_2O_3-xTb_2O_3 (x = 0.00, 1.00, 2.00, 3.00, 4.00, and 5.00 mol%) glasses

exhibit competitive or improved TL properties, indicating their potential use in radiation dosimetry applications.

Table 6. The calculated frequency factor when b is set to 1 and 2.

Glass Codes	S (s^{-1})	
	b=1	b=2
Tb0.0	$3.772x10^{6}$	$3.463x10^{6}$
Tb1.0	$6.760x10^{5}$	$6.200x10^{5}$
Tb2.0	$4.242x10^{5}$	$3.893x10^{5}$
Tb3.0	$6.201x10^{8}$	$5.686x10^{8}$
Tb4.0	1.033	$9.474x10^{1}$
Tb5.0	$2.419x10^{8}$	$2.217x10^{8}$

4. Conclusion

This research investigated the structural, optical, and radiation detection capabilities of boro-tellurite glasses doped with Tb_2O_3. The glass compositions of (30-x) TeO_2: $20B_2O_3$: 20MgO: $10Li_2O$: $10Al_2O_3$: $10La_2O_3$: xTb_2O_3 (x is 0.0, 1.0, 2.0, 3.0, 4.0, and 5.0 mol%) were synthesized using the melt-quenching method. The study revealed significant variations in physical properties, such as density, molar volume, and refractive index, with increasing Tb_2O_3 concentration. XRD analysis confirmed the amorphous nature of the glasses, and FTIR spectroscopy identified characteristic vibrational bands of TeO_3, BO_3, BO_4, and OH groups. Optical absorption spectra showed distinct peaks at 807, 907, 1098, 1281, and 1690 nm, corresponding to Tb^{3+} ion transitions, with absorption intensity increasing proportionally to Tb_2O_3 content. PL studies indicated a peak emission at 545 nm when excited at 486 nm, with the highest intensity observed at a Tb_2O_3 concentration of 4.00 mol%. Further increase in Tb_2O_3 concentration led to concentration quenching, resulting in reduced luminescence intensity. Decay time analysis revealed an exponential decrease with increasing Tb_2O_3 concentrations, indicating a higher rate of non-radiative energy transfer. The CIE1931 color coordinates and color purities confirm the potential of these glasses for green light emission, making them suitable for optical applications. RL, these emission features closely resemble those observed in PL, indicating similar underlying excitation and relaxation mechanisms. TL analysis determined kinetic parameters, including maximum temperature (516.15-527.15 K), activation energy (0.69-1.01 eV), and frequency factor ($3.893x10^{5}$-6.201×10^{8} s^{-1}), calculated using Chen's peak shape method, showcasing the glass's efficient trapping and charge release capabilities. The calculated FOM values were between 1.47% and 2.99%, indicating good FOM compatibility, with only minor deviations in some cases. These findings demonstrate the suitability of Tb_2O_3-doped borotellurite glasses for advanced optical applications, including green light-emitting devices. They also show the effectiveness of these glasses in TLD and radiation detection technologies. This material shows promise as a candidate for future innovations in scintillation and TLD applications.

Acknowledgments

The authors acknowledge Nakhon Pathom Rajabhat University and Thailand Science Research and Innovation (TSRI) for providing the necessary facilities and resources that enabled the successful completion of this study.

References

[1] Mahmoud Hamdy Abaza, A. (2018). New Trend in Radiation Dosimeters. *American Journal of Modern Physics*, *7*(1), 21-30. DOI: 10.11648/j.ajmp.20180701.13.

[2] Sommat, V., Ornketphon, O., Kaewjaeng, S., Kothan, S., Limsuwan P., Thanyaphirak, W., Yasaka, P., Kirdsiri, K., Khondara, S., & Kaewkhao, J. (2004). A novel material for radiation detection

application of zinc bismuth lithium borotellurite glass doped with Dy_2O_3. *Radiation Physics and Chemistry*, *225*, 112108. DOI: 10.1016/j.radphyschem.2024.112108.

[3] West, W. G., & Kearfott, K. J. (2015). Optically Stimulated Luminescence Dosimetry: An Introduction. *Solid State Phenomena*, *238*, 161-173. DOI: 10.4028/www.scientific.net/SSP.238.161.

[4] Kaewkhao, J., Wantana, N., Kaewjaeng, S., Kothan, S., & Kim, H. J. (2016). Luminescence characteristics of Dy^{3+} doped Gd_2O_3-CaO-SiO_2-B_2O_3 scintillating glasses. *Journal of Rare Earths*, *34*(6), 583-589. DOI: 10.1016/S1002-0721(16)60065-0.

[5] Wantana, N., Kaewnuam, E., Damdee, B., Kaewjaeng, S., Kothan, S., Kim, H.J., & Kaewkhao, J. (2018). Energy transfer based emission analysis of Eu^{3+} doped Gd_2O_3-CaO-SiO_2-B_2O_3 glasses for laser and X-rays detection material applications. *Journal of Luminescence*, *194*, 75-81. DOI: 10.1016/j.jlumin.2017.10.004.

[6] Laopaiboon, R., & Bootjomchai, C. (2015). Thermoluminescence studies on alkali-silicate glass doped with dysprosium oxide for use in radiation dosimetry measurement. *Journal of Luminescence*, *158*, 275-280. DOI: 10.1016/j.jlumin.2014.10.017.

[7] Boonin, K., Yasaka, P., Limkitjaroenporn P., Rajaramakrishna R., Askin A., Sayyed M.I., Kothan, S., & Kaewkhao J. (2020). Effect of BaO on lead free zinc barium tellurite glass for radiation shielding materials in nuclear application. *Journal of Non-Crystalline Solids*, *550*, 120386. DOI: 10.1016/j.jnoncrysol.2020.120386.

[8] Yasaka, P., Boonin, K., Duangjai, K., Kim, H. J., Kothan, S., & Kaewkhao, J. (2022). Luminescence, spectroscopic properties and reddish-orange emission from Eu^{3+} ion doped tellurite and fluorotellurite glasses: A comparative study. *Optik*, *265*, 169531. DOI: 10.1016/j.ijleo.2022.169531

[9] Damdee, B., Kirdsiri, K., Kim, H.J., Yamanoi K., Wongdamnern, N., Kidkhunthod, P., Rajaramakrishna, R., & Kaewkhao, J. (2022). Physical and photoluminescence investigations of Eu^{3+} doped gadolinium borate scintillating glass. *Radiation Physics and Chemistry*, *200*, 110386. DOI: 10.1016/j.radphyschem.2022.110386.

[10] Xu, S., Fang, D., Zhang, Z., & Jiang Z. (2005). Effect of OH^- on upconversion luminescence of Er^{3+}-doped oxyhalide tellurite glasses. *Journal of Solid State Chemistry*, *178*, 2159-2162. DOI: 10.1016/j.jssc.2005.03.023.

[11] Rada, S., Culea, M., & Culea, E. (2008). Structure of $TeO_2 \cdot B_2O_3$ glasses inferred from infrared spectroscopy and DFT calculations. *Journal of Non-Crystalline Solids*, *354*(52-54), 5491-5495. DOI: 10.1016/j.jnoncrysol.2008.09.009.

[12] Halimah, M. K., Ami Hazlin, M. N., & Muhammad, F. D. (2018). Experimental and theoretical approach on the optical properties of zinc borotellurite glass doped with dysprosium oxide. *Spectrochimica Acta Part A: Molecular and Biomolecular Spectroscopy*, *195*, 128-135. DOI: 10.1016/j.saa.2017.12.054.

[13] Carnall, W. T., Fields, P. R., & Rajnak, K. (1968). Electronic Energy Levels of the Trivalent Lanthanide Aquo Ions. III. Tb^{3+}. *The Journal of Chemical Physics*, *49*(10), 4447–4449. DOI: 10.1063/1.1669895.

[14] Khrongchaiyaphum, F., Wantana, N., Kaewnuam, E., Pakawanit, P., Phoovasawat, C., Vittayakorn, N., Chanthima, N., Phongsa, A., Intachai, N., Kothan, S., Kim, H.J., & Kaewkhao, J. (2024). Novel Tb^{3+} doped borophosphate glass scintillator for X-ray imaging. *Radiation Physics and Chemistry*, *223*, 111851. DOI: 10.1016/j.radphyschem.2024.111851.

[15] Kesavulu, C. R., Kim, H. J., Lee, S. W., Kaewkhao, J., Kaewnuam, E., & Wantana, N. (2017). Luminescence properties and energy transfer from Gd^{3+} to Tb^{3+} ions in gadolinium calcium silicoborate glasses for green laser application. *Journal of Alloys and Compounds*, *704*, 557-564. DOI: 10.1016/j.jallcom.2017.02.056.

[16] Keskin, İ. Ç., & İlhan, M. (2023). Thermoluminescence Kinetic Parameters and Radioluminescence of RE^{3+} (RE = Pr, Sm, Tb, Ho, Er)-Doped Barium Tantalate Phosphors. *Journal of Electronic Materials*, *52*(8), 5614-5630. DOI: 10.1007/s11664-023-10501-y.

[17] Chen, R. (1969). Chen1969. *Journal of The Electrochemical Society*, 1254-1257.

[18] İlhan, M., & Keskin, İ. Ç. (2020). Evaluation of structural behaviour, radioluminescence, Judd-Ofelt analysis and thermoluminescence kinetic parameters of Eu^{3+} doped TTB–type lead metaniobate phosphor. *Physica B: Condensed Matter*, *585*, 412106. DOI: 10.1016/j.physb.

2020.412106
[19] İlhan, M., Keskin, İ. Ç., & Gültekin, S. (2020). Assessing of Photoluminescence and Thermoluminescence Properties of Dy3+ Doped White Light Emitter TTB-Lead Metatantalate Phosphor. *Journal of Electronic Materials*, *49*(4), 2436-2449. DOI: 10.1007/s11664-020-07939-9.